Pockets of Short-Range Transient Order and Restricted Topological Heterogeneity in the Guanidine-Denatured State Ensemble of GED of Dynamin†

Jeetender Chugh, Shilpy Sharma, and Ramakrishna V. Hosur*

Department of Chemical Sciences, Tata Institute of Fundamental Research, Homi Bhabha Road, Mumbai 400005, India

Received June 29, 2007; Revised Manuscript Received August 13, 2007

ABSTRACT: The nature and variety in the denatured state of a protein, a non-native state under a given set of conditions, has been a subject of intense debate. Here, using multidimensional NMR, we have characterized the 6 M Gdn-HCl-denatured state of GED, the assembly domain of dynamin. Even under such strongly denaturing conditions, we detected the presence of conformations in slow exchange on the NMR chemical shift time scale. Although the GED oligomer as well as the SDS-denatured monomeric GED were seen to be predominantly helical [Chugh et al. (2006) *FEBS J. 273*, 388−397], the 6 M Gdn-HCl-denatured GED has largely β-structural preferences. However, against such a background, we could detect the presence of a population with a short helical stretch (Arg42-Ile47) in the ensemble. The $^1H-^1H$ NOEs suggested presence of pockets of transient short-range order along the chain. Put together these segments may lead to a rather small number of interconverting topologically distinguishable ensembles. Spectral density analysis of ^{15}N relaxation rates and $\{^1H\}-^{15}N$ NOE, measured at 600 and 800 MHz, and comparison of $J(0)$ with hydrophobic patches calculated using AABUF approach, indicated presence of four domains of slow motions. These coincided to a large extent with those showing significant R_{ex}. Additionally, a proline residue in the connection between two of these domains seems to cause a fast hinge motion. These observations help enhance our understanding of protein denatured states, and of folding concepts, in general.

Protein folding, an essential fundamental biological process, can be identified as the "Holy Grail" of biochemistry, as the complete details of this process are not well-understood till date. The elucidation of this process requires the complete characterization of the fully folded native state, the partially folded intermediate states, and the denatured state (*1*−*4*).

Studies about the denatured state(s) of proteins are particularly important, as these are not simply random coils (*5*−*7*) and often possess regions of inhibited flexibility and residual structure (*7*−*9*), which relates to the local preferences within a heterogeneous group of conformers (*10*). In addition, the understanding of these states gains importance because of the evidence of the existence of several intrinsically unstructured biologically functional proteins (*11*, *12*), apart from providing insight about the protein folding mechanism (*2*, *13*, *14*). A close relationship also exists between the partially unfolded equilibrium states (formed at high concentrations of guanidine-HCl, urea, elevated temperature, pH, etc.) and the kinetic intermediates formed during the protein folding process because of the similar principles governing the behavior of proteins (*3*, *4*). These denatured/ unfolded states correspond to the top of the folding funnel, supposed to represent trillions of rapidly interconverting conformations, and it is in these states that the initiation sites for protein folding can be recognized, taking clues from the local preferences represented in the residual structures (*15*, *16*). Thus, the detailed structural and dynamic characterization of these denatured equilibrium states may provide significant contribution to the elucidation of initial events during a folding process (*3*, *4*, *17*, *18*).

The lack of X-ray crystallization data (arising because of crystallization problems) and high-resolution NMR[1] parameters (arising because of a large amount of flexibility in this regime) makes the study of unfolded states all the more challenging. Nevertheless, NMR spectroscopy has been the method of choice in the determination of these structures, as it provides residue-specific conformational data about the denatured proteins (*1*, *4*).

The formation of hydrophobic clusters, usually formed by local side-chain interactions (*7*, *19*−*21*) and the presence of fluctuating secondary structure (*22*−*24*) include the common types of ordering found in denatured proteins generally identified from NMR data such as inter-residual $^1H-^1H$ nuclear Overhauser enhancements (NOEs), ^{15}N R_2 relaxation rates, amide proton temperature coefficients, and backbone nuclei chemical shift information. These residual conformational ordering exhibited by a denatured protein depends mainly on its amino acid sequence; however, variations in ionic concentrations, pH, or crowding changes under the influence of some signals could manipulate the unfolded state.

Unfortunately, the number of NMR reports detailing residue level characterization of the denatured states has been small, and limited to small sized proteins, because of the difficulties in obtaining sequence specific assignments in

† We thank the Government of India for providing financial support to the National Facility of High Field NMR at the Tata Institute of Fundamental Research, India.

* Corresponding author. E-mail: hosur@tifr.res.in, Ph: +91-22-22782271, +91-22-22782488, Fax: +91-22-22804610.

10.1021/bi701280p CCC: $37.00
Published on Web 10/02/2007

these states, and this has hampered unraveling of general concepts governing the denatured sates. Native and non-native type secondary structural preferences have earlier been observed in the urea-denatured state of barstar (*25*), in the guanidine-denatured state of HIV-1 protease (*26*, *27*), and in the acid-denatured state of hUBF HMG Box 1 (*28*). A non-native α-helical structure has been observed in the guanidine-denatured state of β-lactoglobulin, an all β-protein in the native state (*29*). Similarly, β-type preferences have been observed in denatured apomyoglobin, a largely helical protein (*30*). In some cases, multiple types of structures have been reported in the denatured state (*31*−*33*). However, explicit description of the rapid topological changes that occur in the denatured state has remained an impossible task till date.

The GTPase effector domain of dynamin (GED, ≈138 amino acids long) is known to be responsible for the self-assembly of dynamin during its endocytic activity (*34*, *35*). Our earlier results showed that this domain forms very large soluble oligomers in native conditions (*36*). However, in the presence of high concentrations of denaturants including, urea, guanidine, and SDS, it exists largely in the form of a monomer in solution. The oligomer was found to be ∼55% helical, as observed by circular dichroism, and the helical content was fully retained even in the presence of SDS (*36*).

In this study, we used heteronuclear NMR to gain insight about the structural and dynamic properties of 6 M Gdn-HCl-denatured GED. The recently developed triple resonance experiments, HNN and HN(C)N (*37*−*39*), in addition to the conventional experiments, proved extremely successful in obtaining complete resonance assignment. The data presented here demonstrates the presence of pockets of short-range transient order and restricted topological heterogeneity in the Gdn-HCl-denatured state. Some of this order occurs at locations corresponding to predicted secondary structure (mostly α-helical) in the native state (*36*). Furthermore, the dynamics data analyzed with the reduced spectral density functions also identified regions of motional restrictions in the segments that coincided well with those with the hydrophobic stretches on one hand and with the sites of proton-transfer exchange on the other.

EXPERIMENTAL PROCEDURES

Protein Expression and Purification. The cDNA corresponding to the GTPase effector domain (amino acids 618−753) of human dynamin I was subcloned into the BamHI and XhoI sites of the bacterial expression plasmid pGEX4T1 (Amersham Biosciences Corp, Piscataway, NJ). The clone was confirmed by multiple restriction digests and DNA sequencing and then transformed into *Escherichia coli* BL21 cells. Isotopically rich protein samples (^{15}N or ^{15}N and ^{13}C, as required) were prepared using M9 media containing ^{15}-NH_4Cl as the sole source of nitrogen and/or ^{13}C-glucose as the sole source of carbon. The expression of glutathione-S-transferase (GST)-fusion protein was induced with 100 μM of isopropyl-β-D-thiogalactopyranoside for 8 h at 28 °C. The harvested culture was lysed in TEND buffer (20 mM Tris, pH 7.4, 1 mM EDTA, 150 mM NaCl, and 1 mM dithiothreitol) containing lysozyme and routine protease inhibitors. The lysed cells were sonicated and spun at 100 000 g for 45 min to obtain a clear supernatant. The supernatant was incubated with glutathione−sepharose beads (Amersham) for 2 h at 4 °C to allow binding of overexpressed GST-GED recombinant protein. The beads were then washed with TEND buffer. Protein-coated beads were incubated with thrombin (Sigma-Aldrich, St. Louis, MO) for 15 h at 25 °C to remove the GST tag. GST clipping was observed by running samples on 16% SDS-PAGE. The supernatant containing primarily the free GED was then passed over GSH-sepharose column repeatedly to remove any contaminating GST or GST-GED. The protein, thus obtained, had two non-native residues (Gly and Ser) at the N-terminal. Thus the 618th residue of dynamin was actually the third residue in GED, and amino acids in all discussions and figures were numbered accordingly.

The purified protein was finally concentrated to ∼1 mM and exchanged with 10 mM acetate buffer (pH 5.0) containing 1 mM EDTA, 150 mM NaCl, 1 mM DTT, and 6 M Gdn-HCl. The NMR sample was allowed to attain equilibrium before the start of the experiments.

Circular Dichroism. Far-UV CD spectra were recorded at 15 °C on a JASCO J-810 spectropolarimeter (Jasco, Europe). Scans were acquired from 200 to 250 nm with a scan speed of 50 nm/min. A 20 μM protein concentration was used in a quartz cell with a path length of 0.1 cm. The protein samples were equilibrated, with different concentrations of Gdn-HCl, for at least 12 h before recording the experiments. The spectra (for 6 M Gdn-HCl-denatured GED) below 211 nm wavelength were not included for the analysis because of the saturation in that region due to high salt (Gdn-HCl) concentrations.

NMR Spectroscopy. All NMR experiments were performed both on a Varian Inova spectrometer and on a Bruker Avance spectrometer equipped with CryoProbe, operating at ^{1}H frequencies of 600 and 800 MHz, respectively. Both spectrometers were equipped with triple-resonance probes. All the experiments were performed at 15 °C, processed using Felix (Accelrys Software Inc., San Diego, CA) and analyzed using Felix and CARA (*40*). A series of two- and three-dimensional experiments were performed, and HSQC recorded at the end of all these experiments was compared with that recorded at the start, to check the stability of the protein sample under the above-mentioned condition. No change was observed in the series of HSQC spectra, indicating that the protein was stable under the conditions used and it had already reached equilibrium before the start of the experiments. A standard strategy based on heteronuclear triple resonance experiments was used to obtain backbone assignments. HNN, CBCANH, CBCA(CO)NH, HNCO, and HN(CA)CO were used for a sequential walk through the polypeptide chain, and TOCSY−HSQC and NOESY−HSQC were used for assigning the spin systems. Standard experimental parameters used have been listed in Table 2.

Relaxation measurements were done at 600 and 800 MHz. ^{15}N transverse relaxation rates (R_2) were measured with CPMG delays of 10, 30, 50*, 90, 130, 170*, 230, and 300 ms. ^{15}N longitudinal relaxation rates (R_1) were measured with inversion recovery delays of 10, 50, 90, 150*, 300, 500*, 700, and 900 ms, where the points marked with an asterisk were recorded in duplicate. Steady state ^{1}H−^{15}N heteronuclear NOE measurements were carried out with a proton saturation time of 3 s and a relaxation delay of 2 s.

Table 1: Correlation Times (τ) Calculated from Spectral Density Functions

	800 MHz				600 MHz			
	$J(\omega_H)$ vs $J(0)$		$J(\omega_N)$ vs $J(0)$		$J(\omega_H)$ vs $J(0)$		$J(\omega_N)$ vs $J(0)$	
	Fit a	Fit b	Fit a	Fit b	Fit a	Fit b	Fit a	Fit b
α	−0.0681	−0.0057	0.3273	−0.0183	−0.2892	−0.0097	0.7357	0.0139
β (ns/rad)	0.059	0.0203	0.0471	0.269	0.1426	0.0307	−0.0849	0.2425
τ	1.86 ns	54.19 ps, 0.81 ns, 8.04 ns	0.18 ns, 2.54 ns	0.76 ns, 6.3 ns, 29.7 ns	1.01 ns	6.91 ns	2.01 ns	0.65 ns, 8.64 ns

Table 2: Standard Parameters Used for NMR Experiments

NMR parameter	value
TOCSY mixing time	80 ms
NOESY mixing time	150 ms
$N-C^{\alpha}$ and NC' transfer time	24−30 ms
complex increments along ^{15}N dimension	40
complex increments along ^{13}C dimension	48
complex increments along aliphatic ^{13}C dimension	64
complex increments along indirect ^{1}H dimension	96
no. of scans per FID in different experiments	4 to 16

For the experiment without proton saturation, the relaxation delay was 5 s. Amide proton temperature coefficients were measured by recording HSQC spectra from 15 °C to 36 °C at steps of 3 °C. $^3J(H^N-H^{\alpha})$ coupling constants were measured from high-resolution HSQC spectra with 8192 complex t_2 points and 512 complex t_1 points.

In all NMR experiments, ^1H chemical shifts were referenced to HDO [4.598 ppm with respect to 2,2-dimethyl-2-silapentane-5-sulfonic acid (DSS) at 15 °C, 6 M Gdn-HCl, pH 5] while the ^{13}C and ^{15}N chemical shifts were indirectly referenced to DSS.

Spectral Density Functions and Correlation Times. Spectral density functions $J(0)$, $J(\omega_H)$, and $J(\omega_N)$ were calculated as described by Lefevre et al. by the reduced spectral density approach (*41*). The reduced spectral density approach uses only three relaxation parameters, with the assumption that at high frequencies the spectral density functions $J(\omega_H) \approx J(\omega_H + \omega_N) \approx J(\omega_H - \omega_N)$. In this approach, spectral density functions are expressed as follows:

$$J(0) = \frac{3}{2(3d^2 + c^2)}\left[-\frac{1}{2}R_1 + R_2 - \frac{3}{5}R_{NOE}\right] \quad (1)$$

$$J(\omega_N) = \frac{1}{(3d^2 + c^2)}\left[R_1 - \frac{7}{5}R_{NOE}\right] \quad (2)$$

$$J(\omega_H) = \frac{1}{5d^2}R_{NOE} \quad (3)$$

where,

$$R_{NOE} = [(\{^1H\} - {}^{15}N)NOE - 1] \times R_1 \times \left(\frac{\gamma_N}{\gamma_H}\right) \quad (4)$$

The constant c^2 takes the value $\sim 1.25 \times 10^9$ (rad/s)^2 and $\sim 2.25 \times 10^9$ (rad/s)^2 at 600 and 800 MHz magnetic fields, respectively, and the constant d^2 is approximately equal to 1.35×10^9 (rad/s)^2 and is independent of the field strength (*42*). The errors in spectral density functions were calculated, using the above equations, from errors in relaxation parameters, by standard error propagation.

The linear correlation between $J(\omega_H)$ and $J(0)$, and between $J(\omega_N)$ and $J(0)$, was then examined at both the magnetic fields, using the following relation:

$$J(\omega_{H,N}) = \alpha_{H,N}J(0) + \beta_{H,N} \quad (5)$$

α and β thus obtained were used to calculate the correlation times using the following cubic equation:

$$2\alpha_{H,N}\omega_{H,N}{}^2\tau^3 + 5\beta_{H,N}\omega_{H,N}{}^2\tau^2 + 2(\alpha_{H,N} - 1)\tau + 5\beta_{H,N} = 0 \quad (6)$$

The various τ values thus obtained have been listed in Table 1.

RESULTS AND DISCUSSION

Resonance Assignments. The $^1H-^{15}N$ HSQC spectrum of the unfolded GED denatured in 6 M Gdn-HCl at pH 5.7 and 15 °C is depicted in Figure S1. The limited chemical shift dispersion of the resonances (within the range of ~0.75 ppm), particularly in the ^1H dimension, indicated that GED is highly denatured under the experimental conditions. However, the chemical shift dispersion for ^{15}N is large, with relatively well-resolved peaks. Taking advantage of this fact, the assignment of the $^1H-^{15}N$ resonances of GED was carried out mainly using a combination of HNN and HN(C)N experiments (*37*−*39*). Using HNN alone, we were able to assign H^N and ^{15}N for 133 of the 134 non-proline residues (except Glu112) in the denatured state of GED. The patterns around glycine and proline residues in the HNN spectrum provided us with several start points and check points during the sequential walk. An illustrative sequential walk through the segment Ala21-Glu25 is shown in Figure 1. All the assignments thus obtained have been shown in Figure S1. Subsequently, this assignment was verified using the standard multidimensional NMR experiments, including CBCANH, CBCA(CO)NH, HNCO, and HN(CA)CO (*43*) and assignments of all the C^{α}, C^{β}, and C' were obtained in the process. Spin system identification gave further affirmation of the assignments, and during the course of action many of the side chain protons were assigned using TOCSY−HSQC and NOESY−HSQC spectra (*44*).

Slow Conformational Exchange in the Denatured State. Generally, the denatured state is observed as a single average ensemble because of the fact that the polypeptide chain exchanges very rapidly between several conformations. In contrast to this, we observed several additional peaks of low intensity in the HSQC spectra of denatured GED, and a few of these peaks could sequentially be connected to assigned

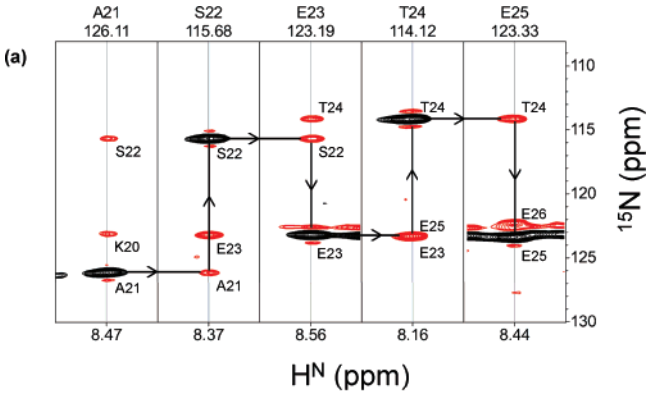

(b) GSASFLRAGVYPERVGDKEKASETEENGSDSFMHSMDPQLERQVE

TIRNLVDSYMAIVNKTVRDLMPKTIMHLMINNTKEFIFSELLANLYSCG

DQNTLMEESAEQAQRRDEMLRMYHALKEALSIIGNINTTTVSTP

FIGURE 1: (a) Sequential walk through the F1−F3 planes of the HNN spectrum of GED in 6 M Gdn-HCl at pH 5 and 15 °C. Sequential connectivities are shown for Ala21 to Glu25 stretch. The F2 (^{15}N) values are shown at the top for each strip. The black and red contours indicate positive and negative peaks. (b) Summary of sequential assignment obtained from the HNN walk along the amino acid sequence of GED. Gly shown in red served as the start/check point while the Pro shown in blue served as the break point.

peaks. It may thus be likely that these additional peaks arise because of the existence of some conformations in slow exchange. For example, the residues (Ala8, Gly9, Val10, Tyr11, Glu13, Met71, and Asp111) were represented by two sets of cross-peaks in the HSQC spectra [Figure 2(a)], which could be sequentially connected; all the unprimed and primed residues are connected within themselves in case of Ala8-Tyr11 [Figure 2(b,c)], and the peaks of Glu13, Met71, and Asp111 are connected with their respective neighbors (data not shown). These observations point toward the presence of some stable structural preferences in the guanidine denatured state ensemble. Interestingly, the primed and the unprimed residues have distinctly different motional characteristics in the sub nanosecond to picoseconds time scale as demonstrated by negative $\{^1H\}-^{15}N$ NOE for unprimed residues and positive $\{^1H\}-^{15}N$ NOEs for primed residues (see later). For the analyses of the denatured state, we have used the unprimed peaks, which represent the majority of the states in the ensemble.

Structural Preferences: All Beta Propensities in an All Alpha-Helical Protein. Chemical shift deviation of H^α, CO, C^α, and C^β (*3*, *45*) from the corresponding random coil values (secondary shifts) act as excellent markers of the conformational propensities present in the polypeptide chain (*1*−*4*, *45*−*48*). However, several sets of random coil values have been reported under different experimental conditions. We calculated the secondary shifts using these different random coil shifts, and the results were found to be largely similar. The dataset determined by Schwarzinger et al. (*49*, *50*) for GGXGG peptides (X = the residue of interest for random coil chemical shift; G = glycine) in 8 M urea and pH 2.3, which includes sequence correction factors for the random coil values was adopted here for a detailed analysis. The secondary shifts calculated using the data set from Wishart et al. (*51*) have been included in the Supporting Information (Figure S2). Among the various studied secondary chemical shifts, those of H^α, C^α, C^β, and CO are of prime importance. While C^α and CO secondary shifts are negative for β-type structures [(ϕ,ψ) = (−70 to −150° and 90 to 180°)], H^α and C^β secondary shifts are positive for the same. The reverse is true if residues have taken (ϕ,ψ) preferences in an α-helical domain [(ϕ,ψ) = (−40 to −80° and −30 to −60°)] of the Ramachandran map.

The sequence-corrected H^α secondary chemical shifts and cumulative (C^α, C^β, and CO) secondary shifts for 6 M Gdn-HCl-denatured GED are plotted in Figure 3(a). The C^{cum} was calculated as:

$$\Delta\delta(C^{cum}) = \Delta\delta(C^\alpha)/25 + \Delta\delta(CO)/10 - \Delta\delta(C^\beta)/25 \quad (7)$$

The normalizations used for the individual secondary shifts in eq 7 are based on the span of the chemical shift of the respective nuclei in folded proteins, and the relative signs of the secondary shifts for the alpha and beta preferences, as discussed above. The pattern of C^{cum} and H^α secondary shifts in the plots indicates that the secondary structure is not random even in the presence of 6 M Gdn-HCl. Although the secondary chemical shift values are small, the overall negative deviations in C^{cum} and the positive deviations in H^α plots for many residues along the chain explains that these residues may have taken up broad β-domain of the (ϕ,ψ) space; this may also include extended conformation and the polyproline II (PP_{II}) structures. A few contiguous stretches [≥3, including Ala3-Arg7, Gln43-Thr46, Ser53-Ala56, Val58-Arg63, Met74-Asn76, Glu80-Ile82, Ala123-Ile126, Asn129-Thr132, and Thr134-Thr137, marked in Figure 3(a)] of negative deviations (>−0.05) in C^{cum} and positive deviations (>0.05) in H^α may indicate conceivable β-structures. The predicted native secondary structure along the length of the protein is shown on the top of Figure 3(a).

Next, $^3J(H^N-H^\alpha)$ coupling constants (J_{obs}) in the denatured GED were measured from the fine structures of the peaks in the HSQC spectrum [representative region shown in Figure 3(c)]. These three bond H^N-H^α coupling constants provide useful insights into the backbone conformational preferences, mainly the ϕ-torsional angles; values range from 3 to 5 Hz for α-helical structures, 8−11 Hz for β-type structures (*45*), and 6−8 Hz for a random coil (J_{random}). The J_{random} values need to be corrected with respect to the sequence context using the factors as determined by Penkett et al. (*52*) for residues preceded by aromatic side chains (class L) or preceded by other residue types (class S). Using these, the secondary coupling constants were calculated as: $J_{obs} - J_{random}$ for 125 of the 133 assigned residues [Figure (3b)]. On analyzing the secondary coupling constants, we found that most of the residues have deviations of <1 Hz from the random coil coupling constant values. It is important to note here that if these secondary coupling constants show negative deviations from random coil values, it indicates helical propensities (this also includes PP_{II} structures) while a positive deviation points toward β-structures. Combining this with secondary chemical shift predictions, one can conclude that for true β type structures, both H^α secondary shifts and $^3J(H^N-H^\alpha)$ secondary couplings would be positive. On the other hand, if the former is positive (such as in β-structures) and the latter is negative (like in common right handed α-helices), it then hints toward the PP_{II} helix (*5*). In the case of Gdn-HCl-denatured GED, a few regions of negative secondary coupling constants were found where the second-

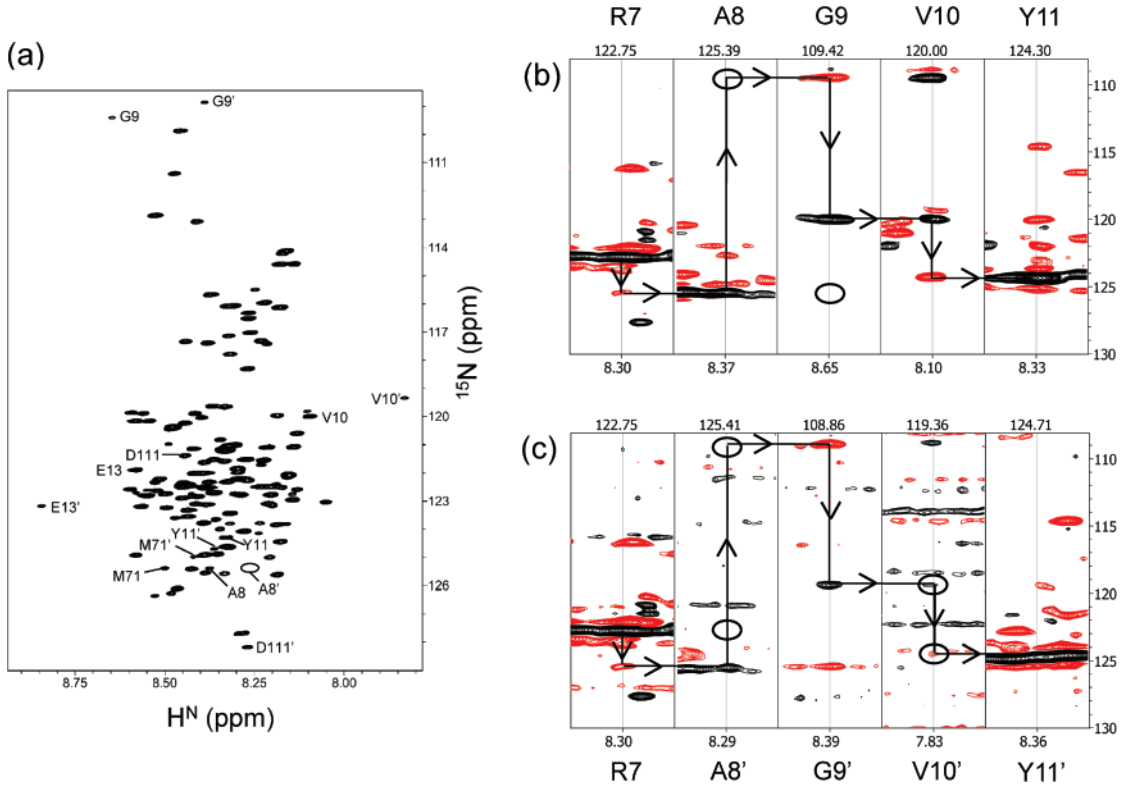

FIGURE 2: (a) $^1H-^{15}N$ HSQC of GED in 6 M Gdn-HCl at pH 5, 15 °C. The residues Ala 8, Gly 9, Val 10, Tyr 11, Glu 13, Met 71, and Asp 111 showing two sets of cross-peaks, and their corresponding counterparts (labeled as primes) have been labeled. All the primed and unprimed residues are connected within themselves in case of Ala8-Tyr11 and the peaks of Glu13, Met 71, and Asp111 to the respective neighbors. Position of Ala 8′ is encircled as the peak is not visible at this contour threshold. Sequential connectivities among the unprimed residues (b) and primed residues (c) is shown though F1−F3 planes of HNN spectrum of GED in 6 M Gdn-HCl at pH 5 and 15 °C. Positions encircled are either not seen in this particular experiment or are very weak at this contour threshold.

ary H^α chemical shift was found to be positive, thus indicating (ϕ,ψ) preference in the the PP_{II} region. A residue-wise evaluation was performed and regions of probable β-structures and the PP_{II} helix, based on combination of secondary chemical shifts and secondary coupling constants, are tabulated in Supporting Information Table S1.

PP_{II} structures in the chemically denatured states of proteins have been reported earlier and have been characterized by the presence of a positive CD band at 225 nm (*5*, *53*−*58*); the (ϕ,ψ) values for these structures lie within the broad β-domain in the Ramachandran plot. However, we failed to detect any positive band at 225 nm in the circular dichroism spectra of GED in 6 M Gdn-HCl at pH 5 and 15 °C [Figure 3(d)]. In addition to this, the absence of any contiguous stretch (≥4 residues) of PP_{II} helix [as analyzed using the $^3J(H^N-H^\alpha)$ secondary coupling constants] indicated the formation of only a transient rather than a stable structure of this type.

Further, the residue-wise amide proton temperature coefficients were estimated by following the chemical shifts of backbone amide protons in Gdn-HCl-denatured GED from 15 °C to 36 °C. In general, the amide proton temperature coefficients can provide valuable information about hydrogen bonding interactions and solvent sequestration in unfolded proteins. If the value of these coefficients is more positive than −4.5 ppb/K, the residue is said to be involved in H-bonding (*59*). In our case, the measured temperature coefficients (Figure S3) values ranged from −6.53 ppb/K to −10.09 ppb/K, thereby hinting toward the absence of H-bonds formation in the Gdn-HCl-denatured state of GED.

All these observations collectively suggest the absence of any stable structure in the Gdn-HCl-denatured state of GED. However, most residues show (ϕ,ψ) preferences in the β-domain of Ramachandran map, and a few residues fall in the regions belonging to PP_{II} structures. This is important in the following background (*36*): (a) the GED oligomer is largely helical, (b) SDS denaturation breaks the oligomer into monomers, but the helical character of the chain is completely preserved, and (c) the polypeptide chain has intrinsic preferences for the helical structure as seen by prediction algorithms. Thus the present observation of largely β-preferences would have significant implication for the folding mechanism of the protein, since the protein switches to totally non-native structural preferences near the surface of the folding funnel.

Backbone Dynamics and Topological Fluctuations in the Denatured State. The backbone dynamics of the Gdn-HCl-denatured GED were investigated with ^{15}N R_1 (longitudinal relaxation rate), ^{15}N R_2 (transverse relaxation rate), and $\{^1H\}-^{15}N$ heteronuclear NOE data recorded at 600 and 800 MHz spectrometer frequencies. These data are sensitive to motions on a range of time scales. While the R_1 and $\{^1H\}-^{15}N$ heteronuclear NOE are largely sensitive to fast motions (ns-ps time scale), the R_2 is sensitive to low-frequency motions (ms-μs time scale) and reflects contributions from slower exchange processes.

The relaxation rates were determined for 108 (on 600 MHz) and 116 (on 800 MHz) out of the 133 assigned residues. The R_1values ranged from 1.32 to 2.19 s^{-1} [average being 1.79 (± 0.06) s^{-1}] at 600 MHz frequency and 1.29 to

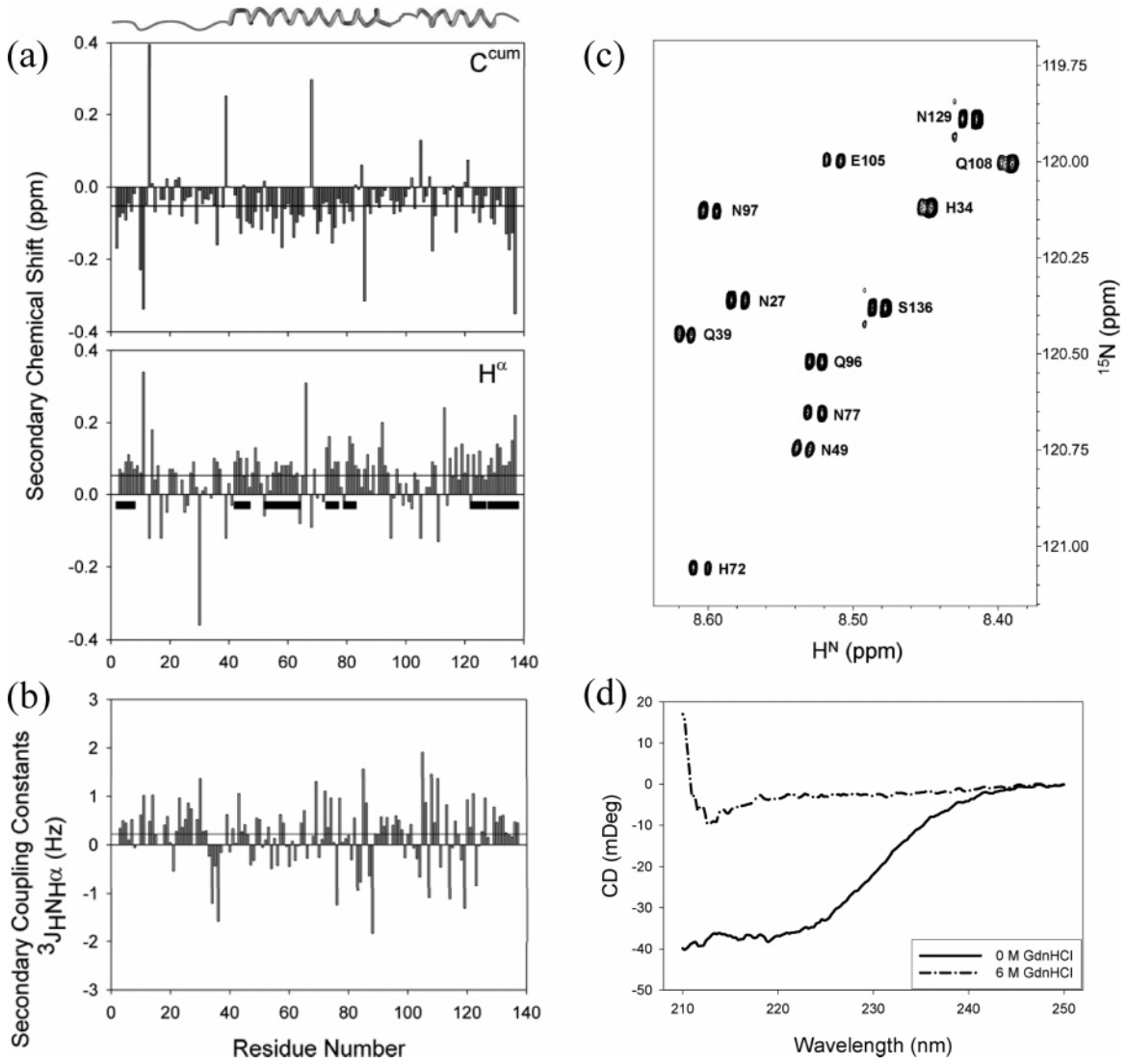

FIGURE 3: (a) Plots of C^{cum} and H^{α} sequence-corrected (see text) secondary chemical shifts for GED in 6 M Gdn-HCl at pH 5 and 15 °C. Sequence-corrected random coil values, as determined by Schwarzinger et al. (*49*, *50*), have been used. The average values, −0.05 for C^{cum} and 0.05 for H^{α}, are represented with a horizontal line while the predicted native secondary structure elements are shown on top of the plots (*36*). The black bars in the H^{α} plot indicates the contiguous stretches [≥3] of negative deviations (>−0.05) in C^{cum} and positive deviations (>0.05) in H^{α}. (b) Secondary coupling constants $^3J(H^N-H^{\alpha})$ plotted against residue numbers, as calculated from high resolution $^1H-^{15}N$ HSQC of GED. The average value (0.22 Hz) is indicated by a horizontal line. (c) Selected region of the high resolution $^1H-^{15}N$ HSQC to show the quality of the spectral resolution. Splitting in the peaks was used to measure the $^3J(H^N-H^{\alpha})$ coupling constants. (d) Far-UV circular dichroism spectra of GED at pH 5 and 15 °C, in the absence of Gdn-HCl (full line) and in presence of 6 M Gdn-HCl (dashed line).

2.38 s^{-1} [average being 1.68 (± 0.06) s^{-1}] on 800 MHz frequency [Figure 4(a)]. The $\{^1H\}-^{15}N$ NOE values also showed a wide variation [Figure 4(c)] on both spectrometer frequencies [values ranged from −2.13 to +0.44 on 600 MHz and −0.66 to +0.71 on 800 MHz, respectively]. These NOE values were considerably lower than +0.82, the expected value for NH groups of a rigid globular protein that is tumbling isotropically (*60*), thereby clearly indicating flexibility throughout the Gdn-HCl-denatured GED. Similarly, a considerable variation was observed in the R_2 values, which ranged from 2.06 to 6.72 s^{-1} [average being 4.56 (± 0.21) s^{-1}] at 600 MHz frequency and 2.54 to 8.99 s^{-1} [average being 5.88 (± 0.21) s^{-1}] on 800 MHz frequency [Figure 4(b)]. It would be important to note here that all the values for all the three relaxation parameters were less in the first 15 residues of the polypeptide chain (with negative $\{^1H\}-^{15}N$ NOE values for a few of them), thereby indicating increased conformational flexibility in this region. Even so, the primed and the unprimed residues in the stretch Ala8-Glu13 seemed to have different $\{^1H\}-^{15}N$ NOE characteristics. For example, Gly9′ = +0.58, Gly9 = −0.67; Val10′ = +0.49, Val10 = −0.32. This indicates occurrence of partially ordered conformations in the N-terminal in the ensemble.

Further, the nonuniformity of the R_2/R_1 ratio [Figure 4(d)] demonstrates the presence of a significant nonrandom structure in the Gdn-HCl-denatured GED. Such nonrandom structures have also been reported in the urea-unfolded states of several other proteins (*7*, *9*, *61*, *62*) and for natively unfolded proteins (*63*, *64*). As can be seen from Figure 4(d), there are four peaks in the pattern which represent distinct clusters of residues [marked as A (Glu13-Glu26), B (His34-Met66), C (Asn76-Leu90), and D (Met100-Ala123)]. Of these, B, C, and D domains largely belong to those regions where secondary structures (mostly α-helical) were predicted in the native state (*36*). It would be important to note that

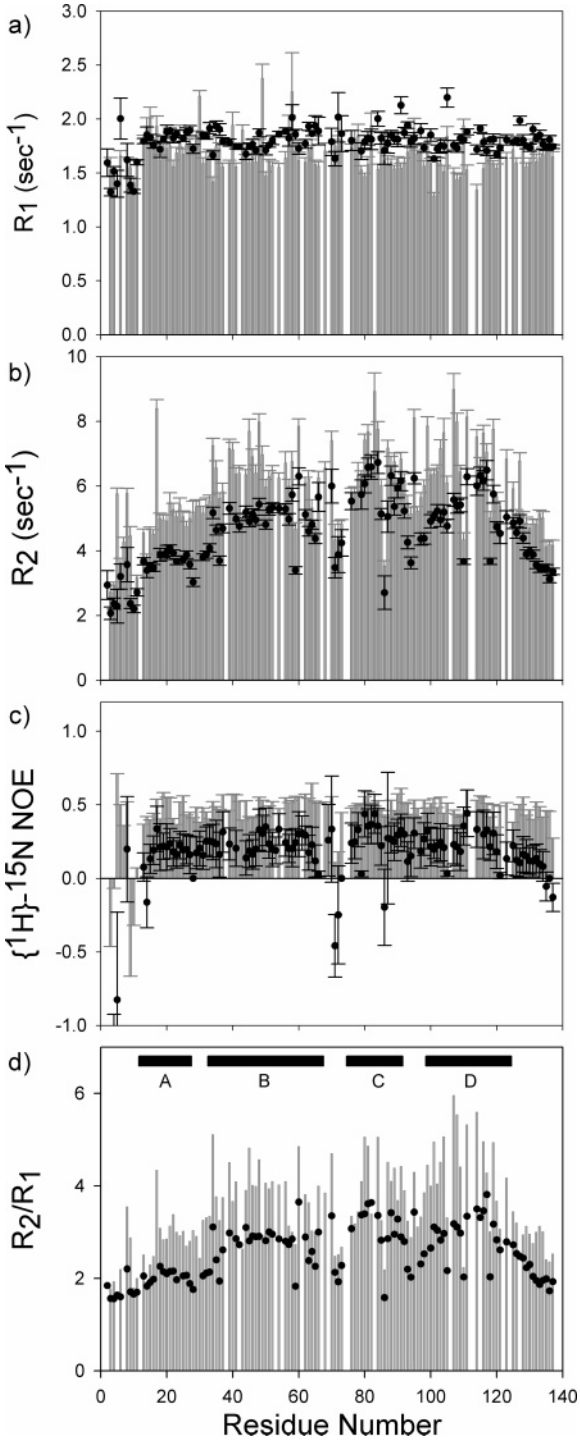

FIGURE 4: Relaxation parameters from 600 MHz (filled circles) and 800 MHz (vertical bars) versus the residue number for 6 M Gdn-HCl-denatured GED in 10 mM acetate buffer at pH 5.0 and 15 °C: (a) ^{15}N R_1 (longitudinal relaxation rate), (b) ^{15}N R_2 (transverse relaxation rate), (c) $\{^1H\}-^{15}N$ heteronuclear NOE and d) R_2/R_1 with black bars [marked as A (Glu 13-Glu 26), B (His 34-Met 66), C (Asn 76-Leu 90), and D (Met 100-Ala 123)] representing areas of significant nonrandom structures.

the regions Gln43-Thr46, Ser53-Ala56, and Val58-Arg63 (part of B) and Met74-Asn76 and Glu80-Ile82 (part of C) showed β-propensities from the sequence-corrected secondary chemical shifts calculations [Figure 3(a)].

The relaxation data, collected on both 600 and 800 MHz spectrometer frequencies, was next analyzed using the reduced spectral density method. The spectral density functions $J(0)$, $J(\omega_N)$, and $J(\omega_H)$ were calculated (*41*, *65*) (as explained in Experimental Procedures), and their residue-wise variations are plotted in Figure 5. The values for $J(\omega_N)$ (largely determined by R_1) remain similar all across the polypeptide chain, except at the N terminal, where the values are diminished. $J(\omega_H)$, largely determined by heteronuclear NOE, exhibited a greater degree of variation with larger values at the N-terminus and in the middle of the molecule (residues Met71 and His72), as depicted in Figure 5(a). This relative increase in fast motions at the N-terminus is a characteristic feature of denatured proteins. It would be interesting to note here that the residues Met71 and His72, in the middle of the polypeptide chain, contribute to fast motions [Figure 5(a)] without a concomitant contribution to intermediate time scale motions [Figure 5(b)]. This increase in motion could be attributed to the presence of Pro67, known to enhance flexibility, in the vicinity of these residues.

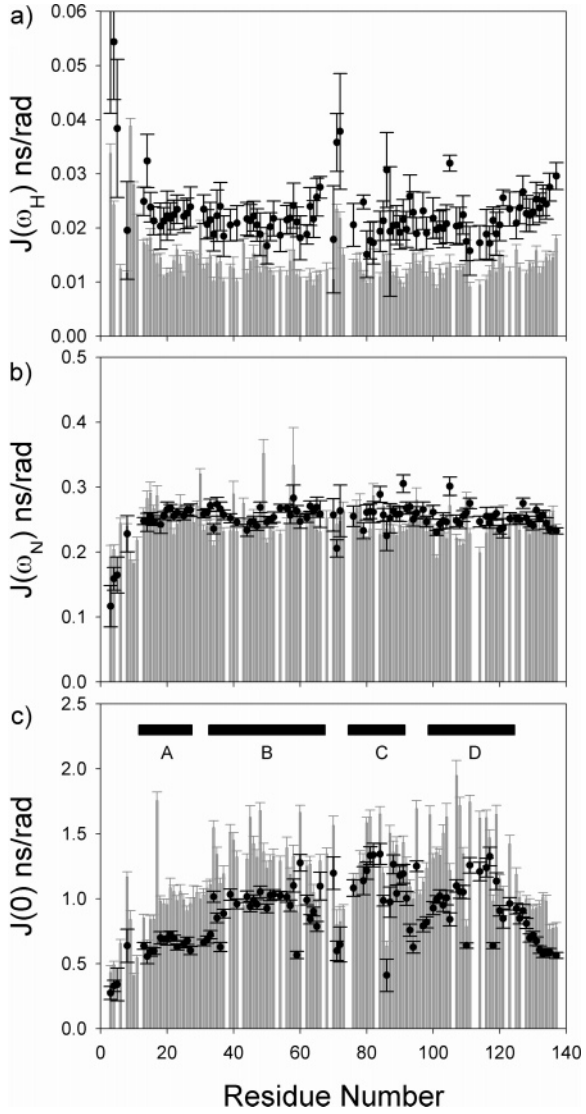

FIGURE 5: Calculated values of spectral density functions from relaxation data at 600 MHz (filled circles) and 800 MHz (vertical bars): (a) $J(\omega_H)$, (b) $J(\omega_N)$, and (c) $J(0)$ versus residue numbers. The black bars indicate the regions with reduced flexibility [marked as A (Glu 13-Glu 26), B (His 34-Met 66), C (Asn 76-Leu 90), and D (Met 100-Ala 123)] in the polypeptide chain.

The spectral density at zero frequency, $J(0)$, is largely dictated by R_2 and since the value of R_2 is increased because of the contribution from chemical exchange (R_{ex}), artifactual

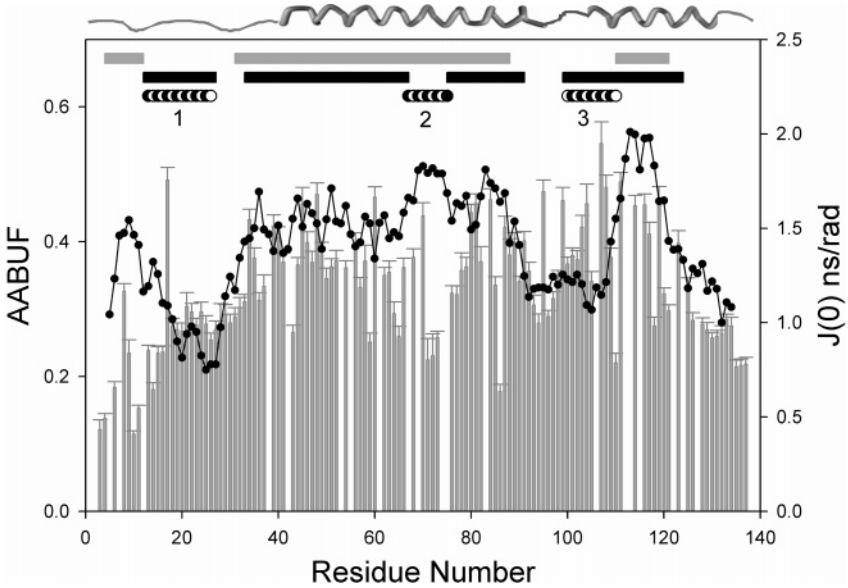

FIGURE 6: Plots of calculated $J(0)$ values at 800 MHz (vertical bars) and AABUF (average area buried upon folding, filled circles) for 6 M Gdn-HCl-denatured GED. The AABUF values were calculated with the ExPASy tool ProtScale [http:// www.us.expasy.org/tools/protscal.html]. The predicted secondary structure (*36*) is shown on the top of the figure. The regions with increased AABUF values and reduced flexibility [as identified from Figures 4(d) and 5(c), respectively] and have been marked with gray and black bars on the top, respectively. Stretches, where AABUF profile does not match with $J(0)$ values, have been marked as patterned strips 1, 2, and 3.

increase in $J(0)$ values can be observed. Figure 5(c) shows the values of $J(0)$ calculated from relaxation data at both 600 and 800 MHz. In either case, there is a substantial unevenness along the polypeptide sequence. This matches closely with the variations in R_2 [Figure 4(b)]. The regions with higher $J(0)$ values [regions A, B, C, and D; Figure 5(c)] indicate the regions with contributions from slow chemical exchange in the polypeptide chain.

Further insights into the dynamics of the ordered regions of polypeptide were obtained by analyzing the correlation between transverse relaxation behavior and average area buried upon folding (AABUF[1]), a parameter developed by Rose et al. (*66*). The AABUF is proportional to the hydrophobic contribution of a residue to the conformational free energy of a protein, and it has been shown to correlate well with sequence-dependent dynamic variations due to cluster formation in case of urea-denatured apomyoglobin (*7*) and the natively unfolded translocation domain of colicin E9 (*63*). Interestingly, the AABUF profile (marked as gray strips, Figure 6) was found to emulate the $J(0)$ plots (marked as black strips, Figure 6) and at least three distinct regions with reduced flexibility [namely, B, C, and a part of D identified from $J(0)$ analysis; Figure 4(d) and Figure 5(c)] were found to correspond with regions with increased AABUF values and hence increased hydrophobic content. This would indicate the presence of local hydrophobic interactions in these regions. However, three regions were identified in the polypeptide chain where the AABUF profile and the $J(0)$ values did not match (marked as patterned strips, Figure 6). These included the A region (residues Glu13-Glu26; Figure 6, stretch 1), region between B and C (Lys68-Ile75; Figure 6, stretch 2) and first half of D (residues Tyr91-Arg110; Figure 6, stretch 3). It would be important to note here that there are 1 Asp and 4 Glu residues in stretch 1 while there are 1 Asp and 3 Glu in stretch 3. The pK_a values of the side chains of Asp and Glu are $\approx$4.0 and 4.4−4.5, respectively, and all our experiments have been recorded at pH 5.0. Thus, the differences in these two profiles may be attributed to the chemical exchange that may occur in the side chains of these charged residues at this pH. This chemical exchange would induce local conformational exchange, since the changes in the charge state would alter the electrostatic potential and thus the conformations. On the other hand, the region between B and C (Lys68-Ile75; Figure 6, stretch 2) was associated with high AABUF values while the $J(0)$ values for the same were low. This difference could be attributed to the presence of a Pro67 in this region, a residue known to enhance flexibility. The analysis of the spectral density function $J(\omega_N)$ also pointed toward a similar observation as discussed earlier.

Correlation times, reflecting different kinds of motions exhibited by the polypeptide chain, were calculated from the linear fit equations between the spectral densities $J(\omega_{N,\,H})$ with $J(0)$ (Figure 7) (as described in Experimental Procedures). The parameters from the regression analysis and the correlation times (only real and positive roots were considered), thus derived, have been tabulated in Table 1. Values ranging from a few nanoseconds to as high as $\approx$29 ns were observed. These possibly reflect the distribution of the overall tumbling motions which can happen because of the different topologies of the members of the ensemble. On the other hand, correlation time values below 1.0 ns were also observed, which might correspond to the local motions in the molecule. In addition to this, two domains of linear fits (Fit a and Fit b, Figure 7) were identified at 600 as well as 800 MHz frequency using the $J(\omega_H)$ and $J(\omega_N)$ vs $J(0)$ plot, thus pointing toward some distinct regions of different mobilities along the polypeptide chain in denatured GED. The residues Ala3, Ser4, Leu6, Val10, Tyr11, and Arg14 [as identified from 800 MHz; fit a, Figure 7(a)], and the

[1] Abbereviations: AABUF, average area buried upon folding; NMR, nuclear magnetic resonance; HSQC, heteronuclear single quantum coherence; GED, GTPase effector domain; CD, circular dichroism; $\{^1H\}-^{15}N$ NOE, heteronuclear NOE; SDS, sodium dodecyl sulfate.

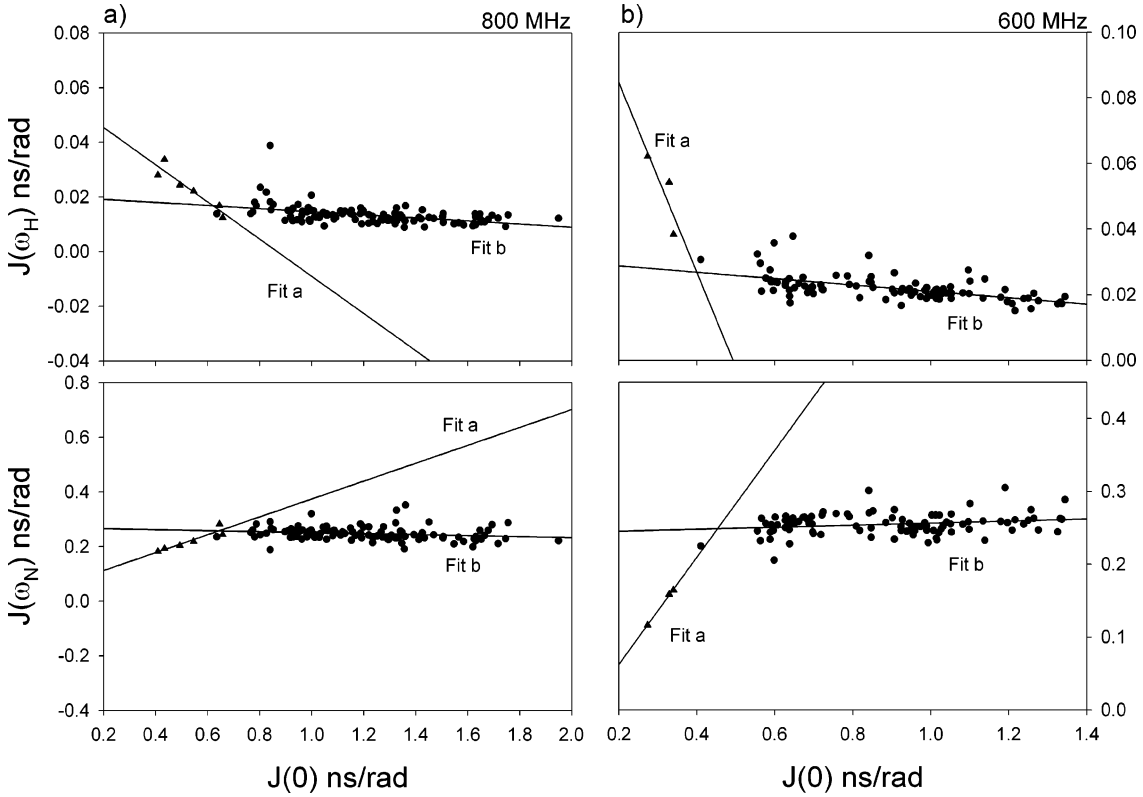

FIGURE 7: The spectral density functions $J(\omega_H)$ and $J(\omega_N)$ are plotted against $J(0)$ at two field strengths: (a) 600 MHz, and (b) 800 MHz. Plots were fitted as per empirical relation between the spectral density functions: $J(\omega_{H,N}) = \alpha_{H,N}J(0) + \beta_{H,N}$. The plots at both the fields show two domains of linear fit, fit a and fit b. Various α and β values and the τ values (see text) thus obtained have been tabulated (Table 1).

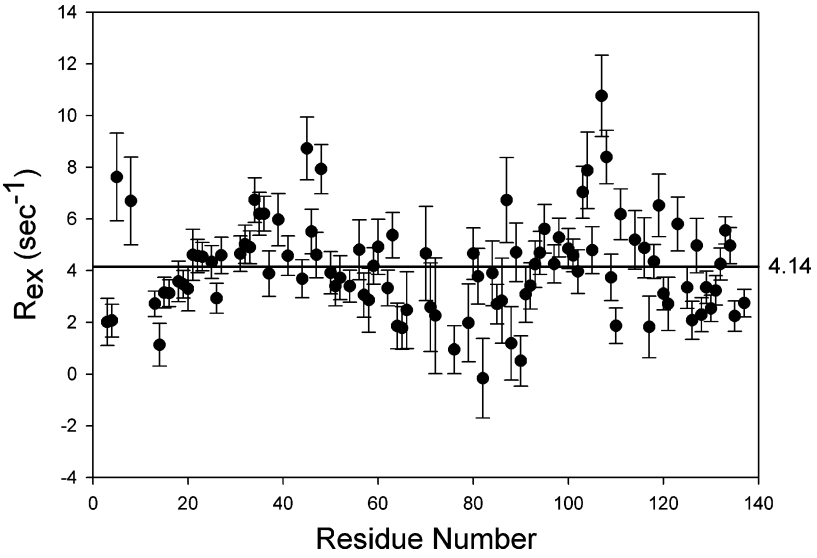

FIGURE 8: Residue-wise R_{ex} values at $\omega_N = 81.1$ MHz as calculated from spectral density functions $J(0)$ at two field strengths, 600 and 800 MHz. The horizontal line indicates the average value (4.14 s^{-1}).

residues Ala3, Ser4, and Phe5 [as identified from 600 MHz; fit a, Figure 7(b)], formed one region of different mobility while the rest of the residues formed the other.

An exchange on ms-μs time scale contributes to the observed transverse relaxation rates ($R_2 = R_{2,int} + R_{ex}$, where $R_{2,int}$ is the intrinsic rate, R_2 is the observed rate and R_{ex} is the contribution from slow exchange). Thus, the measurement of R_{ex} provides a means to assess slow topological fluctuations in the ensemble. However, inputs from R_1, R_2, and $^1H-^{15}N$ NOE at a minimum of two fields are required for the measurement of R_{ex} (*67*). The residue-wise R_{ex} values for any ω_N can be calculated using the following equation:

$$R_{ex}(\omega_N) = {\omega_N}^2 \cdot \frac{[J(0)]_{800MHz} - [J(0)]_{600MHz}}{\lambda_{800MHz}{\omega_{N,800MHz}}^2 - \lambda_{600MHz}{\omega_{N,600MHz}}^2} \quad (8)$$

and presently the values for $\omega_N = 81.1$ MHz (^1H frequency, 800 MHz) are shown in Figure 8, where $\lambda = 3/[2(3d^2 + c^2)]$, the constant c^2 takes the value $\sim 1.25 \times 10^9$ (rad/s)^2 and $\sim 2.25 \times 10^9$ (rad/s)^2 at 600 and 800 MHz magnetic fields, respectively, and the constant d^2 is approximately

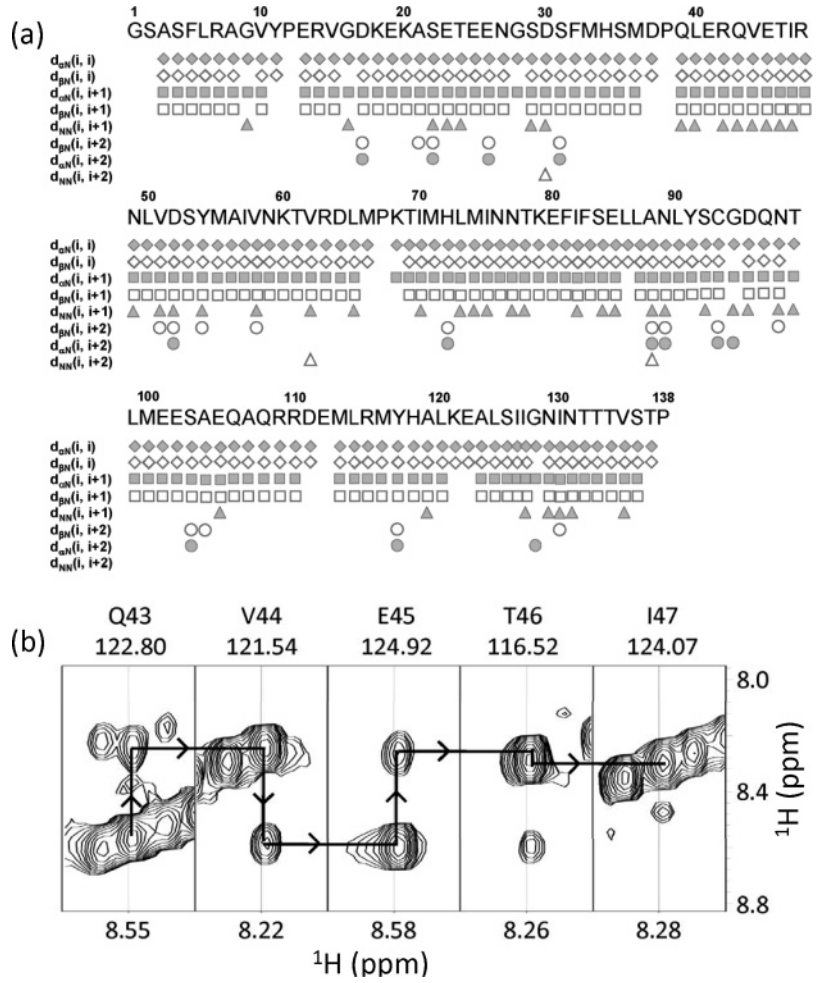

FIGURE 9: (a) Summary of ^{1}H−^{1}H sequence specific connectivities as observed using a three-dimensional ^{15}N edited NOESY−HSQC spectrum for GED in 6 M Gdn-HCl at pH 5.0, 15 °C. (b) Gln 43 to Ile 47 strips from the amide region of 3D- NOESY HSQC spectrum with mixing time 150 ms in 6 M Gdn-HCl-denatured GED. The sequential residues have been connected with arrows. The numbers at the top indicate ^{15}N chemical shifts.

equal to 1.35×10^9 (rad/s)^2 and is independent of the field strength (*42*), while the details of $J(0)$ values are plotted in Figures 5. As can been seen from the figure, most residues do exhibit some contribution from slow conformational exchange to the relaxation rates, though a significant variation was observed in the contributions at the different residue sites. This is not surprising since we detected presence of some conformations in slow exchange on the NMR chemical shifts time scale [Figure 2(a)]. Clearly, there can be conformations exchanging on variety of time scales and this could vary along the sequence.

Slow conformational exchanges in the denatured states have been reported in the past, and this particularly happens, when, under the given experimental conditions some partially ordered structures prevail in the ensemble [reviewed in (*68*)].

In conclusion, the data suggest that the Gdn-HCl-denatured GED lacks a regular secondary structure, has propensity for β-structures and exists as a dynamic ensemble of species that contain clusters of locally interacting residues, which contain both aromatic and aliphatic side chains. Some of these clusters are hydrophobic in nature while others are charged.

Pockets of Short-Range Transient Order: Implications for GED Folding. ^{1}H−^{1}H NOEs have the potential to throw light on the nature of the topological preferences in the denatured ensemble, since they depend on the occurrence of short interproton distances (<5 Å). The NOE intensity will be a weighted average, and thus if there is a population containing a conformation with a particular short distance, then a characteristic NOE will show up. Thus, while the secondary shifts highlight the sequence-wise (ϕ,ψ) preferences in the major population of the ensemble, the ^{1}H−^{1}H NOEs can help detect the presence of certain specific topologies, even if they belong to a minor population. The $d_{\alpha N}$ (i, $i + 1$), $d_{\beta N}$ (i, $i + 1$) and d_{NN} (i, $i + 1$) interproton distances are less than 5 Å, irrespective of the (ϕ,ψ) combinations, and these NOEs are expected in an ensemble with rapidly interconverting structures. Virtually all denatured states show sequential $d_{\alpha N}$ (i, i+ 1) and $d_{\beta N}$ (i, $i + 1$) NOEs because of extensive conformational averaging and greater tendency to populate the β-region of the (ϕ,ψ) space (*69*). On the other hand, sequential d_{NN} (i, $i + 1$) NOEs would be observed only if there is a population of α-helical conformations in the ensemble.

Therefore, to gain further insight about the topological preferences in the Gdn-HCl-denatured state of GED, a three-dimensional ^{15}N edited NOESY−HSQC was performed. Figure 9(a) shows the summary of all the observed connectivities. While, $d_{\alpha N}$ (i, $i + 1$) and $d_{\beta N}$ (i, $i + 1$) NOEs were observed almost throughout the sequence, 45 d_{NN} (i, $i + 1$)

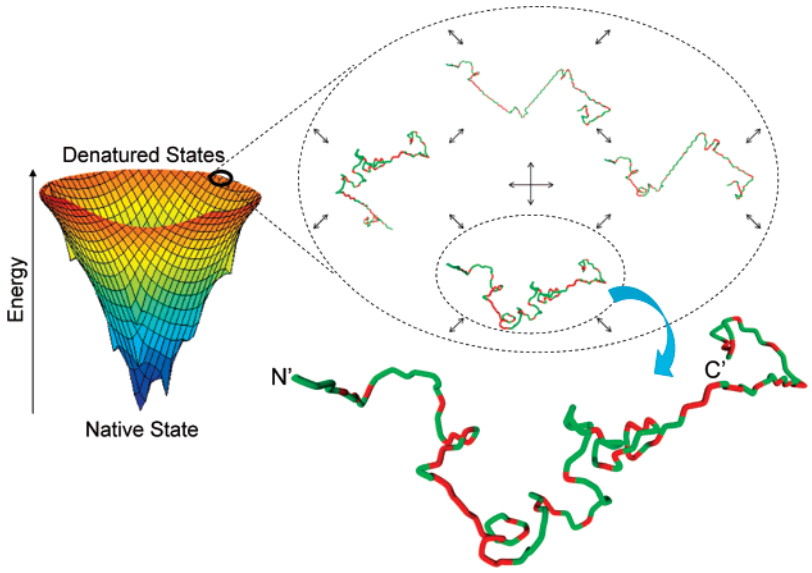

FIGURE 10: Representation of a few of the topologies, generated using ProteinShop (*71*), which contain the turn and helical propensities at a few residues as seen from the $^1H-^1H$ NOE data. One of the topology is magnified to show the areas with high (above average value, Figure 8) R_{ex} (marked red). Equilibrium is shown among various species. The protein folding funnel is also shown to emphasize that these topologies belong to denatured state.

NOEs were observed, thereby pointing toward the fact that the backbone fluctuates over both α and β regions of the (ϕ,ψ) space in several regions. All these interproton distances are less than 5 Å, irrespective of the (ϕ,ψ) combinations, and these NOEs are expected in an ensemble with rapidly interconverting structures. However, it is interesting to note that the segment comprising of amino acids Arg42-Ile47 shows a continuous stretch of sequential d_{NN} (i, i + 1) NOE connectivities, thereby suggesting that the Gdn-HCl denatured state of GED samples a relatively stable short structure in this region [Figure 9(b)]. Incidentally, this region constitutes a part of the first long helix predicted by the secondary structure prediction algorithms on the basis of amino acid sequence (*36*), which suggests that, indeed, this may fold into a helix under native conditions. However, this α-propensity was not observed in the secondary chemical shift analysis, possibly because of its low population. The residues Arg42-Val44 showed up as β-type conformation, thereby pointing toward the existence of heterogeneous population in the denatured ensemble.

Even though, the spectra did not show any long-range NOEs, a few short-range (i, i +2) NOEs were detected [Figure 9(a)], constituting a total of 18 $d_{\beta N}$ (i , i +2), 13 $d_{\alpha N}$ (i , i +2), and 3 d_{NN} (i , i +2), thereby indicating toward the presence of some short-range order along the sequence, perhaps transiently, in the ensemble. Further, since these NOEs were observed at a few locations only, it suggested the influence of the sequence in dictating such a short-range order. It is interesting to note that both $d_{\beta N}$ (i, i +2) and $d_{\alpha N}$ (i, i +2) NOEs were observed for at least 11 residues [Figure 9(a)], thereby hinting toward the possibility of populations which have a turn (type II) among different (ϕ,ψ) combinations of nearby residues, at these locations along the polypeptide chain. Each of these turns could represent an ensemble with a short-range order. We may mention here that the β-representative secondary shifts which cover a wide range of (ϕ,ψ) combinations in the Ramachandran plot would encompass the β-turn conformations as well. Although any single one of the turns may not be readily distinguishable from the random structure population, combinations of a few of them would create distinguishable topologies for the chain. The possibility of the presence of only 11 such turns, as hypothesized from the earlier observations, in a 138 residue long protein further restricts the number of topologies in the ensemble than imagined otherwise. This has an important implication for the folding mechanism of the protein. Since each one of the topologies could form a starting point for the folding of the protein to its native state when appropriate folding conditions (e.g., dilution of the denaturant) are provided, and since the number of topologies appears to be rather small, it emerges that the number of folding pathways would also be rather small for the protein.

Next, to visualize some of the members with the preferred topologies in the ensemble, a few of them were created by assigning the most favored (ϕ,ψ) torsion angle values in the Ramachandran map to the individual residues, as per their β-, α-, and turn propensities [Figure 3 and Figure 9(a)]. Figure 10 depicts a few of those topologies which contained the turn and helical propensities at few residues as seen in the NOE data, the rest being in β-conformation. We hasten to add here that the shown structures are based on propensities and represent only a small fraction of the population in the ensemble. Interestingly, these contain some collapsed structures at a few places, and they coincide with regions showing significant R_{ex} values (Figure 10, marked red). In other words, the significant occurrence of R_{ex} at several sites could, thus, be attributed to the occurrence of topological fluctuations among the preferred ones in the ensemble. To emphasize that these structures belong to the denatured state ensemble at the top of the folding funnel, Figure 10 also shows the folding funnel. The possible causes of such structural collapses were further analyzed, and a few of these topologies were found to contain either hydrophobic and/or nonpolar residues in the collapsed areas. This is in accordance with the hydrophobic clusters predicted from the $J(0)$ and AABUF analysis performed above, and as also reported in earlier observations in denatured states (*7*, *19*−*21*). Such clusters have also been observed in recent Monte Carlo

simulations of the denatured ensembles (*70*). We envisage that other kinds of structures driven by electrostatic interactions between the side chains could also be visible in some other topologies, not represented here.

In conclusion, using multidimensional NMR, we have successfully investigated here the guanidine-denatured state of GED, the assembly domain of dynamin, involved in dynamin oligomerization during endocytosis. Our data presented here indicates toward the existence of multiple conformations in slow exchange as represented by the presence of dual peaks in HSQC at a few sites along the polypeptide chain. In addition, even in the presence of 6 M Gdn-HCl, the secondary structure is not random and there exist pockets of short-range transient order with restricted topological heterogeneity. Also, the guanidine-denatured state of GED exhibited structural preferences in the broad β-domain of the Ramachandran map, in contrast to the native structure which is mostly α-helical. In addition to this, several residues over the length of the protein were found to populate polyproline II type structure in the denatured state. We could also observe 11 turn-like propensities at various positions in the polypeptide length. Considering that combinations of these features could result in distinguishable topologies, it appears that there are possibly only a small number of topologies interconverting in the denatured state. Furthermore, the Gdn-HCl-denatured state of GED was found to exhibit motional restrictions largely in those regions where secondary structures (mostly α-helical) were predicted in the native state. These structural and motional characteristics in the denatured state could have an influence on the folding pathways of the protein; there are perhaps only a small number of pathways as can be judged from the fact that there are only a small number of topologies, each one of which can be a folding nucleus, in the denatured ensemble. The results also indicate that the presence of native structural preferences in the denatured state is not a necessary condition for a protein to fold. Thus, the results presented here, while providing the structural and dynamics characteristics of the Gdn-HCl-denatured state of GED, help to enhance our understanding of denatured states and of folding concepts, in general.

ACKNOWLEDGMENT

We thank Dr. Rohit Mittal for the GED clone and help in protein preparation. J.C. acknowledges Fred Damberger for all the help provided for learning the software CARA. The authors acknowledge Surender Chugh for the development of software for calculating sequence-dependent correction factors using dataset determined by Schwarzinger et al. Discussions with Atul K Srivastava during graphic preparation are deeply acknowledged.

SUPPORTING INFORMATION AVAILABLE

Table S1 presents residue-wise structural preferences based on CSI-H^{α} and secondary coupling constants. Figures S1, S2, and S3 illustrates the residue specific assignment marked on $^{1}H-^{15}N$ HSQC spectra of GED, secondary chemical shifts as calculated using values from Wishart et al., and a residue-wise plot of temperature coefficients for GED in 6 M Gdn-HCl, respectively. This material is available free of charge via the Internet at http://pubs.acs.org.

REFERENCES

1. Shortle, D. R. (1996) Structural analysis of non-native states of proteins by NMR methods, *Curr. Opin. Struct. Biol. 6*, 24−30.
2. Dyson, H. J., and Wright, P. E. (1998) Equilibrium NMR studies of unfolded and partially folded proteins, *Nat. Struct. Biol. 5 Suppl*, 499−503.
3. Dyson, H. J., and Wright, P. E. (2001) Nuclear magnetic resonance methods for elucidation of structure and dynamics in disordered states, *Methods Enzymol. 339*, 258−270.
4. Dyson, H. J., and Wright, P. E. (2004) Unfolded proteins and protein folding studied by NMR, *Chem. Rev. 104*, 3607−3622.
5. Kumar, A., Srivastava, S., Mishra, R. K., Mittal, R., and Hosur, R. V. (2006) Local structural preferences and dynamics restrictions in the urea-denatured state of SUMO-1: NMR characterization, *Biophys. J. 90*, 2498−2509.
6. Religa, T. L., Markson, J. S., Mayor, U., Freund, S. M., and Fersht, A. R. (2005) Solution structure of a protein denatured state and folding intermediate, *Nature 437*, 1053−1056.
7. Schwarzinger, S., Wright, P. E., and Dyson, H. J. (2002) Molecular hinges in protein folding: the urea-denatured state of apomyoglobin, *Biochemistry 41*, 12681−12686.
8. Klein-Seetharaman, J., Oikawa, M., Grimshaw, S. B., Wirmer, J., Duchardt, E., Ueda, T., Imoto, T., Smith, L. J., Dobson, C. M., and Schwalbe, H. (2002) Long-range interactions within a nonnative protein, *Science 295*, 1719−1722.
9. Le Duff, C. S., Whittaker, S. B., Radford, S. E., and Moore, G. R. (2006) Characterisation of the conformational properties of urea-unfolded Im7: implications for the early stages of protein folding, *J. Mol. Biol. 364*, 824−835.
10. Smith, L. J., Fiebig, K. M., Schwalbe, H., and Dobson, C. M. (1996) The concept of a random coil. Residual structure in peptides and denatured proteins, *Fold. Des 1*, R95−106.
11. Wright, P. E., and Dyson, H. J. (1999) Intrinsically unstructured proteins: re-assessing the protein structure-function paradigm, *J. Mol. Biol. 293*, 321−331.
12. Eliezer, D. (2007) Characterizing residual structure in disordered protein States using nuclear magnetic resonance, *Methods Mol. Biol. 350*, 49−67, 49−67.
13. Rose, G. D., Fleming, P. J., Banavar, J. R., and Maritan, A. (2006) A backbone-based theory of protein folding, *Proc. Natl. Acad. Sci. U.S.A. 103*, 16623−16633.
14. Dill, K. A., and Shortle, D. (1991) Denatured states of proteins, *Annu. Rev. Biochem. 60*, 795−825.
15. Dinner, A. R., Sali, A., Smith, L. J., Dobson, C. M., and Karplus, M. (2000) Understanding protein folding via free-energy surfaces from theory and experiment, *Trends Biochem. Sci. 25*, 331−339.
16. Daggett, V., and Fersht, A. R. (2003) Is there a unifying mechanism for protein folding, *Trends Biochem. Sci. 28*, 18−25.
17. Brockwell, D. J., Smith, D. A., and Radford, S. E. (2000) Protein folding mechanisms: new methods and emerging ideas, *Curr. Opin. Struct. Biol. 10*, 16−25.
18. Ptitsyn, O. B. (1995) Structures of folding intermediates, *Curr. Opin. Struct. Biol. 5*, 74−78.
19. Hodsdon, M. E., and Frieden, C. (2001) Intestinal fatty acid binding protein: the folding mechanism as determined by NMR studies, *Biochemistry 40*, 732−742.
20. Lietzow, M. A., Jamin, M., Jane Dyson, H. J., and Wright, P. E. (2002) Mapping long-range contacts in a highly unfolded protein, *J. Mol. Biol. 322*, 655−662.
21. Neri, D., Billeter, M., Wider, G., and Wuthrich, K. (1992) NMR determination of residual structure in a urea-denatured protein, the 434-repressor, *Science 257*, 1559−1563.
22. Arcus, V. L., Vuilleumier, S., Freund, S. M., Bycroft, M., and Fersht, A. R. (1995) A comparison of the pH, urea, and temperature-denatured states of barnase by heteronuclear NMR: implications for the initiation of protein folding, *J. Mol. Biol. 254*, 305−321.
23. Wong, K. B., Clarke, J., Bond, C. J., Neira, J. L., Freund, S. M., Fersht, A. R., and Daggett, V. (2000) Towards a complete description of the structural and dynamic properties of the denatured state of barnase and the role of residual structure in folding, *J. Mol. Biol. 296*, 1257−1282.
24. Serrano, L., Matouschek, A., and Fersht, A. R. (1992) The folding of an enzyme. VI. The folding pathway of barnase: comparison with theoretical models, *J. Mol. Biol. 224*, 847−859.

25. Bhavesh, N. S., Juneja, J., Udgaonkar, J. B., and Hosur, R. V. (2004) Native and nonnative conformational preferences in the urea-unfolded state of barstar, *Protein Sci. 13*, 3085−3091.
26. Bhavesh, N. S., Panchal, S. C., Mittal, R., and Hosur, R. V. (2001) NMR identification of local structural preferences in HIV-1 protease tethered heterodimer in 6 M guanidine hydrochloride, *FEBS Lett. 509*, 218−224.
27. Bhavesh, N. S., Sinha, R., Mohan, P. M., and Hosur, R. V. (2003) NMR elucidation of early folding hierarchy in HIV-1 protease, *J. Biol. Chem. 278*, 19980−19985.
28. Zhang, X., Xu, Y., Zhang, J., Wu, J., and Shi, Y. (2005) Structural and dynamic characterization of the acid-unfolded state of hUBF HMG box 1 provides clues for the early events in protein folding, *Biochemistry 44*, 8117−8125.
29. Hamada, D., and Goto, Y. (1997) The equilibrium intermediate of beta-lactoglobulin with non-native alpha-helical structure, *J. Mol. Biol. 269*, 479−487.
30. Mohana-Borges, R., Goto, N. K., Kroon, G. J., Dyson, H. J., and Wright, P. E. (2004) Structural characterization of unfolded states of apomyoglobin using residual dipolar couplings, *J. Mol. Biol. 340*, 1131−1142.
31. Crowhurst, K. A., Tollinger, M., and Forman-Kay, J. D. (2002) Cooperative interactions and a non-native buried Trp in the unfolded state of an SH3 domain, *J. Mol. Biol. 322*, 163−178.
32. Crowhurst, K. A., and Forman-Kay, J. D. (2003) Aromatic and methyl NOEs highlight hydrophobic clustering in the unfolded state of an SH3 domain, *Biochemistry 42*, 8687−8695.
33. Mok, K. H., and Han, K. H. (1999) NMR solution conformation of an antitoxic analogue of alpha-conotoxin GI: identification of a common nicotinic acetylcholine receptor alpha 1-subunit binding surface for small ligands and alpha-conotoxins, *Biochemistry 38*, 11895−11904.
34. Okamoto, P. M., Tripet, B., Litowski, J., Hodges, R. S., and Vallee, R. B. (1999) Multiple distinct coiled-coils are involved in dynamin self-assembly, *J. Biol. Chem. 274*, 10277−10286.
35. Sever, S., Muhlberg, A. B., and Schmid, S. L. (1999) Impairment of dynamin's GAP domain stimulates receptor-mediated endocytosis, *Nature 398*, 481−486.
36. Chugh, J., Chatterjee, A., Kumar, A., Mishra, R. K., Mittal, R., and Hosur, R. V. (2006) Structural characterization of the large soluble oligomers of the GTPase effector domain of dynamin, *FEBS J. 273*, 388−397.
37. Bhavesh, N. S., Panchal, S. C., and Hosur, R. V. (2001) An efficient high-throughput resonance assignment procedure for structural genomics and protein folding research by NMR, *Biochemistry 40*, 14727−14735.
38. Panchal, S. C., Bhavesh, N. S., and Hosur, R. V. (2001) Improved 3D triple resonance experiments, HNN and HN(C)N, for HN and 15N sequential correlations in (13C, 15N) labeled proteins: application to unfolded proteins, *J. Biomol. NMR 20*, 135−147.
39. Chatterjee, A., Bhavesh, N. S., Panchal, S. C., and Hosur, R. V. (2002) A novel protocol based on HN(C)N for rapid resonance assignment in ((15)N, (13)C) labeled proteins: implications to structural genomics, *Biochem. Biophys. Res. Commun. 293*, 427−432.
40. Keller, R. (2004) *The Computer Aided Resonance Assignment Tutorial CANTINA*, Verlag, Goldau, Switzerland.
41. Lefevre, J. F., Dayie, K. T., Peng, J. W., and Wagner, G. (1996) Internal mobility in the partially folded DNA binding and dimerization domains of GAL4: NMR analysis of the N-H spectral density functions, *Biochemistry 35*, 2674−2686.
42. Zhang, P., Dayie, K. T., and Wagner, G. (1997) Unusual lack of internal mobility and fast overall tumbling in oxidized flavodoxin from Anacystis nidulans, *J. Mol. Biol. 272*, 443−455.
43. Ferentz, A. E., and Wagner, G. (2000) NMR spectroscopy: a multifaceted approach to macromolecular structure, *Q. Rev. Biophys. 33*, 29−65.
44. Fesik, S. W., and Zuiderweg, E. R. (1990) Heteronuclear three-dimensional NMR spectroscopy of isotopically labelled biological macromolecules, *Q. Rev. Biophys. 23*, 97−131.
45. Dyson, H. J., and Wright, P. E. (2002) Insights into the structure and dynamics of unfolded proteins from nuclear magnetic resonance, *Adv. Protein Chem. 62*, 311−340.
46. Wishart, D. S., Sykes, B. D., and Richards, F. M. (1991) Relationship between nuclear magnetic resonance chemical shift and protein secondary structure, *J. Mol. Biol. 222*, 311−333.
47. Wishart, D. S., and Sykes, B. D. (1994) Chemical shifts as a tool for structure determination, *Methods Enzymol. 239*, 363−392.
48. Wishart, D. S., and Sykes, B. D. (1994) The 13C chemical-shift index: a simple method for the identification of protein secondary structure using 13C chemical-shift data, *J. Biomol. NMR 4*, 171−180.
49. Schwarzinger, S., Kroon, G. J., Foss, T. R., Wright, P. E., and Dyson, H. J. (2000) Random coil chemical shifts in acidic 8 M urea: implementation of random coil shift data in NMRView, *J. Biomol. NMR 18*, 43−48.
50. Schwarzinger, S., Kroon, G. J., Foss, T. R., Chung, J., Wright, P. E., and Dyson, H. J. (2001) Sequence-dependent correction of random coil NMR chemical shifts, *J. Am. Chem. Soc. 123*, 2970−2978.
51. Wishart, D. S., Bigam, C. G., Holm, A., Hodges, R. S., and Sykes, B. D. (1995) 1H, 13C and 15N random coil NMR chemical shifts of the common amino acids. I. Investigations of nearest-neighbor effects, *J. Biomol. NMR 5*, 67−81.
52. Penkett, C. J., Redfield, C., Dodd, I., Hubbard, J., McBay, D. L., Mossakowska, D. E., Smith, R. A., Dobson, C. M., and Smith, L. J. (1997) NMR analysis of main-chain conformational preferences in an unfolded fibronectin-binding protein, *J. Mol. Biol. 274*, 152−159.
53. Jha, A. K., Colubri, A., Freed, K. F., and Sosnick, T. R. (2005) Statistical coil model of the unfolded state: resolving the reconciliation problem, *Proc. Natl. Acad. Sci. U.S.A. 102*, 13099−13104.
54. Kelly, M. A., Chellgren, B. W., Rucker, A. L., Troutman, J. M., Fried, M. G., Miller, A. F., and Creamer, T. P. (2001) Host-guest study of left-handed polyproline II helix formation, *Biochemistry 40*, 14376−14383.
55. Moyna, G., Williams, H. J., Nachman, R. J., and Scott, A. I. (1999) Detection of nascent polyproline II helices in solution by NMR in synthetic insect kinin neuropeptide mimics containing the X-Pro-Pro-X motif, *J. Pept. Res. 53*, 294−301.
56. Parrot, I., Huang, P. C., and Khosla, C. (2002) Circular dichroism and nuclear magnetic resonance spectroscopic analysis of immunogenic gluten peptides and their analogs, *J. Biol. Chem. 277*, 45572−45578.
57. Shi, Z., Woody, R. W., and Kallenbach, N. R. (2002) Is polyproline II a major backbone conformation in unfolded proteins, *Adv. Protein Chem. 62*, 163−240.
58. Tremmel, P., and Geyer, A. (2002) An oligomeric ser-pro dipeptide mimetic assuming the polyproline II helix conformation, *J. Am. Chem. Soc. 124*, 8548−8549.
59. Baxter, N. J., and Williamson, M. P. (1997) Temperature dependence of 1H chemical shifts in proteins, *J. Biomol. NMR 9*, 359−369.
60. Kay, L. E., Torchia, D. A., and Bax, A. (1989) Backbone dynamics of proteins as studied by 15N inverse detected heteronuclear NMR spectroscopy: application to staphylococcal nuclease, *Biochemistry 28*, 8972−8979.
61. Klein-Seetharaman, J., Oikawa, M., Grimshaw, S. B., Wirmer, J., Duchardt, E., Ueda, T., Imoto, T., Smith, L. J., Dobson, C. M., and Schwalbe, H. (2002) Long-range interactions within a nonnative protein, *Science 295*, 1719−1722.
62. McCarney, E. R., Kohn, J. E., and Plaxco, K. W. (2005) Is there or isn't there? The case for (and against) residual structure in chemically denatured proteins, *Crit. Rev. Biochem. Mol. Biol. 40*, 181−189.
63. Tozawa, K., Macdonald, C. J., Penfold, C. N., James, R., Kleanthous, C., Clayden, N. J., and Moore, G. R. (2005) Clusters in an intrinsically disordered protein create a protein-binding site: the TolB-binding region of colicin E9, *Biochemistry 44*, 11496−11507.
64. Donne, D. G., Viles, J. H., Groth, D., Mehlhorn, I., James, T. L., Cohen, F. E., Prusiner, S. B., Wright, P. E., and Dyson, H. J. (1997) Structure of the recombinant full-length hamster prion protein PrP(29−231): the N terminus is highly flexible, *Proc. Natl. Acad. Sci. U.S.A. 94*, 13452−13457.
65. Peng, J. W., and Wagner, G. (1992) Mapping of the spectral densities of N-H bond motions in eglin c using heteronuclear relaxation experiments, *Biochemistry 31*, 8571−8586.
66. Rose, G. D., Geselowitz, A. R., Lesser, G. J., Lee, R. H., and Zehfus, M. H. (1985) Hydrophobicity of amino acid residues in globular proteins, *Science 229*, 834−838.

67. Wong, K. B., Fersht, A. R., and Freund, S. M. (1997) NMR 15N relaxation and structural studies reveal slow conformational exchange in barstar C40/82A, *J. Mol. Biol. 268*, 494−511.
68. Dyson, H. J., and Wright, P. E. (1996) Insights into protein folding from NMR, *Annu. Rev. Phys. Chem. 47*, 369−395.
69. Dyson, H. J., and Wright, P. E. (1991) Defining solution conformations of small linear peptides, *Annu. Rev. Biophys. Biophys. Chem. 20*, 519−538.
70. Vendruscolo, M., Paci, E., Karplus, M., and Dobson, C. M. (2003) Structures and relative free energies of partially folded states of proteins, *Proc. Natl. Acad. Sci. U.S.A. 100*, 14817−14821.
71. Crivelli, S., Kreylos, O., Hamann, B., Max, N., and Bethel, W. (2004) ProteinShop: a tool for interactive protein manipulation and steering, *J. Comput.-Aided Mol. Des. 18*, 271−285.

BI701280P